Int. J. Electrochem. Sci., 15 **(2020)** 3578 – 3592, doi: 10.20964/2020.04.45

International Journal of
ELECTROCHEMICAL
SCIENCE
www.electrochemsci.org

EIS measurements on porous cell stacks with an $La_{0.85}Sr_{0.15}Co_xMn_{1-x}O_3$ (x=0, 0.01, 0.03 and 0.05) - $Ce_{0.9}Gd_{0.1}O_{1.95}$ backbone in an atmosphere containing NO_x

R. M. L. Werchmeister, K. Kammer Hansen

Department of Energy Conversion and Storage, Technical University of Denmark
*E-mail: kkha@dtu.dk

Received: 17 December 2019 / *Accepted:* 20 January 2020 / *Published:* 10 March 2020

Ceramic porous cell stacks with electrodes made of $La_{0.85}Sr_{0.15}Co_xMn_{1-x}O_3$ - $Ce_{0.9}Gd_{0.1}O_{1.95}$ (x=0, 0.01, 0.03, and 0.05) were analyzed using electrochemical impedance spectroscopy. Some of the cells were infiltrated with BaO and one was infiltrated with both BaO and $La_{0.85}Sr_{0.15}MnO_3$. Most of the tests were performed in 10% O_2 in Ar with or without 1000 ppm of NO between 250 and 500 °C. The polarization resistance was lower for the cell stacks infiltrated with BaO than for the backbone structure, indicating that the BaO nanoparticles increased the activity of the electrodes. Additional infiltration with $La_{0.85}Sr_{0.15}MnO_3$ also decreased the resistance. Doping $La_{0.85}Sr_{0.15}Mn_{1-y}Co_yO_{3+d}$ (LSCoM) with Co affects the impedance spectra, increasing the resistance of the electrolyte as the Co doping level increases, possibly due to segregation of the Co to the triple phase boundary. In contrast, the resistances of the middle- and low-frequency arcs decrease with increasing Co content. Thus, the electrodes are more active at reducing NO_x when 3 or 5% Co is doped into the B-site.

Keywords: DeNOx, EIS, infiltration, NOx reduction, electrochemical cell

1. INTRODUCTION

As legislation on diesel exhaust becomes ever stricter, there is an ongoing search for new ways to lower the emission of NO_x (=NO and NO_2), particulate matter (PM), CO, and hydrocarbons. Currently, particle filters are used for removing PM, and selective catalytic reduction (SCR) is applied to reduce NO_x levels. However, SCR technologies are stressed by new demands from legislation and suffer from drawbacks such as: dependence on a reducing agent, more complicated technology as the reducing agent should be precisely dosed and safely stored on a moving vehicle. Another applied technology for deNO_x is NO_x storage and reduction (NSR) [1], which is mainly used in Japan due to its vulnerability to any sulfur in the fuel. Two major disadvantages of this technology are the necessity of careful engine control and the need for reducing periods where the engine has to run with a low air-to-

fuel ratio that lowers the fuel efficiency. In this study, we focused on another, less explored, method for the removal of NO_x and other elements from diesel exhaust which does not require a reducing agent or periodically running the engine at lower fuel efficiencies. Electrochemical exhaust gas purification uses an electrochemical cell to reduce NO_x at the cathode, forming N_2, and transport oxide ions through the electrolyte to form O_2 at the anode. This concept was first introduced by Pancharatnam [2] in 1975 where NO was reduced with Pt electrodes on a zirconia disc. Later, Cicero [3] proved that NO could be reduced electrochemically in the presence of O_2. Since then, several other studies have been made in this field [4-10].

In this work, we studied solid oxide electrochemical cells with $Ce_{0.9}Gd_{0.1}O_{1.95}$ (CGO10) electrolytes and composite electrodes of $La_{0.85}Sr_{0.15}Co_xMn_{1-x}O_3$(LSCoM) - CGO10 where the B sites of LSCoM were doped with various concentrations of Co (x=0, 0.01, 0.03 and 0.05). The investigated cells are, in fact, porous cell stacks, and the exhaust gas is pressed through the pores of the ceramic cells. This type of cell stack has been investigated before [11,12] as the design provides good contact between the gas molecules and the electro-catalyst. Furthermore, the concept could be expanded to also oxidize PM, trapped in the large pores of the cell stack and oxidized to CO_2.

The cell stacks are infiltrated with BaO and $La_{0.85}Sr_{0.15}MnO_3$ (LSM15) to increase the activity. Traulsen *et al.* [12] found that infiltration with BaO increased the activity of the conversion of NO in the presence of O_2. LSM has been proven to be active in the electrochemical reduction of NO [5] and the infiltration with LSM might increase the activity of the electrode since the ceramic backbone structure loses substantial activity due to the coarsening that occurs during high-temperature sintering.

The backbone structure was doped with Co to increase the activity of the electrodes. LSCoM has been proposed as a good candidate for IT-SOFCs [13] and it is therefore an interesting electrode material for electrochemical exhaust gas cleaning as the operating temperatures in this field are even lower than for IT-SOFCs. Furthermore, LSCoM should have better ionic conductivity than LSM [12].

In this study, the porous cell stacks are characterized with electrochemical impedance spectroscopy (EIS) at 250–500 °C in atmospheres including 10% O_2 in Ar, 1000 ppm NO + 10% O_2 in Ar, and 1000 ppm NO_2 + 10% O_2 in Ar. Cyclic voltammetry, polarization studies and gas analysis have been reported elsewhere [15]. An EIS study is used to identify which processes substantially affect the polarization resistance (R_p). For this analysis, we recorded a large number of impedance spectrograms, varying experimental conditions, including the atmosphere, temperature, and polarization of the electrode.

2. EXPERIMENTAL

The LSCoM powder was synthesized using the glycine nitrate synthesis [16] and then calcinated at 900 °C. The phase purity of the metal oxide powder was confirmed using powder X-ray diffraction on a Bruker diffractometer. The precursor metal nitrates for the glycine nitrate combustion synthesis were purchased from Alfa Aesar, and the CGO10 powder from Rohdia.

The porous cell stacks were produced by tape casting layers of electrodes and electrolyte. The electrode slurries were made from LSCoM/LSM15 and CGO10 powder, binder, solvent and pore former,

and the electrolyte slurries were made from CGO10 powder, binder, solvent, and pore-former. Graphite powder and poly(methyl methacrylate) (PMMA) were used as pore-formers as these two can, in combination, form a network of small channels and larger pores that is perfect for moving the gas through the cell stack.

The cell stacks were infiltrated with BaO by immersing the whole cell stack in a 0.32 M solution of $Ba(NO_3)_2$ in Millipore water with a surfactant for 10 minutes under vacuum. This was followed by heat treatment at 700 °C for 1 hour to form BaO nanoparticles. This step was repeated until a load of 1.5 to 2 wt% of BaO infiltration was achieved. Some of the cell stacks were also infiltrated with LSM15 which was accomplished by immersing the cell stack into a solution of the metal nitrate precursors for LSM15 (0.7 M) in Millipore water under vacuum and subsequently heating the cell stack to 500 °C. As LSM15 has electronic conductivity and the liquid penetrates into the porous electrolyte, this treatment was only conducted once to minimize the risk of short circuiting.

The cell stacks consist of 11 alternating layers of electrodes and electrolyte which makes 5 whole cells. The top and bottom electrode layers were painted with gold paste with 20 wt% graphite as a current collector and then the cell stacks were mounted in an experimental setup between two alumina tubes containing probes with working and counter electrodes. A further description of cell stack and setup is available in our previous work [15]. The setup was enclosed in a glass tube inside a vertical furnace which allows the temperature to be controlled. Gas was led to the cell stack through the alumina tubes at a rate of 33 mL/min provided by Brooks mass flow controllers. Most of the experiments were conducted in an atmosphere of 1000 ppm NO + 10% O_2 in Ar or 10% O_2 in Ar as reference. A small series of experiments were conducted with varying concentrations of NO (500, 1000 and 2000 ppm).

The experiments were conducted between 250 and 500 °C at 50 degrees intervals.

Most of the impedance spectra were measured at OCV with an amplitude of 36 mV RMS. Measurements taken under polarization are clearly indicated where they are presented. The maximum frequency was 1 MHz and the minimum frequency was 100 mHz.

Before the EIS spectra were fitted with equivalent circuits, a Kramers-Kronig test was used to evaluate the consistency of the experimental data.

The impedance spectra were deconvoluted using *Equivalent Circuit for Windows* [17] from the University of Twente. Ideally, the impedance spectra consists of a serial resistance (R_s) and RC subunits where C is a capacitor. In reality, it is more suitable to use a constant phase element (Q) as defined in equation 1 [18]:

$$Q = 1/(Y_0(j\omega)^n) \quad (1)$$

In equation 1, Y_0 is the amplitude of the constant phase element admittance, j is the imaginary unit, ω is the angular frequency, and n is the frequency exponent.

The constant phase element is dependent on the frequency and therefore the equivalent capacitance, C_ω, is used instead to compare the capacitances, equation 2 [17].

$$C_\omega = R^{(1-n)n}Y_0^{1/n} \quad (2)$$

It was sought to obtain a reasonable fit with an Rs with the least number of RQ units. First the fitting of the EIS spectra was compared to identify common processes and calculate average n-values suitable for another round of fitting.

A Zeiss Supra 35 scanning electron microscope (SEM) was used to examine the cell stacks. Prior to SEM imaging, the cells were broken and the cross section was investigated.

3. RESULTS

The cell stacks were examined with SEM before and after the testing. The 11 alternating layers of electrodes and electrolyte were all very porous, and no delamination was detected. The BaO nanoparticles could easily be found on the surface of the infiltrated cell stacks prior to testing. The BaO particles mainly occupied the LSM phase and their concentration was higher on the outer layers of the cell stack than in the inner layers. For further details, see the previous report that includes SEM images [15].

3.1. Impedance measurements

It was necessary to use 2–4 arcs to model the measured impedance depending on the temperature, gas composition and electrode composition. The impedance spectra were fitted with an equivalent circuit of R_s connected in series with 2–4 subunits consisting of a resistance in parallel with an equivalent capacitance (RQ).

Generally, only equivalent circuits above 400 °C contained 4 RQ elements while below 400 °C, the spectra could be modelled with only two RQ elements. The measurements at 250 °C were shifted substantially towards the low-frequency range and large parts of the measurements were missing, the impedance arc did not contact the real axis in the low-frequency range. Therefore, only the values for R_s and the first, clearly distinguishable high-frequency arc were included in the calculation of the activation energy (E_a) and the equivalent capacitance (EC) range for measurements at 250 °C.

3.2. Backbone

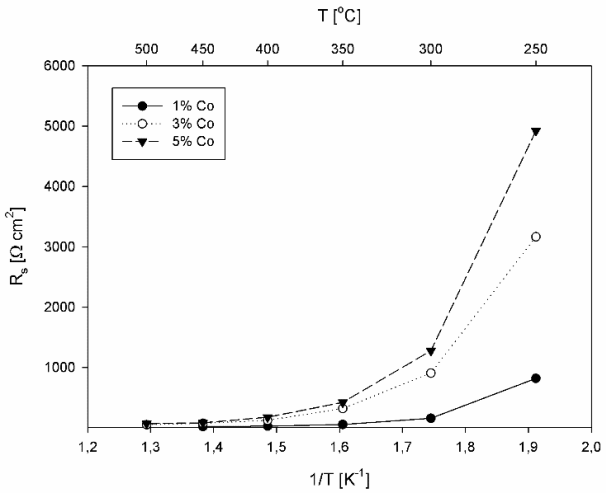

Figure 1. Series resistance of the backbone at 250–500 °C in 10% O_2 in Ar for the cells with LSCoM/CGO electrodes.

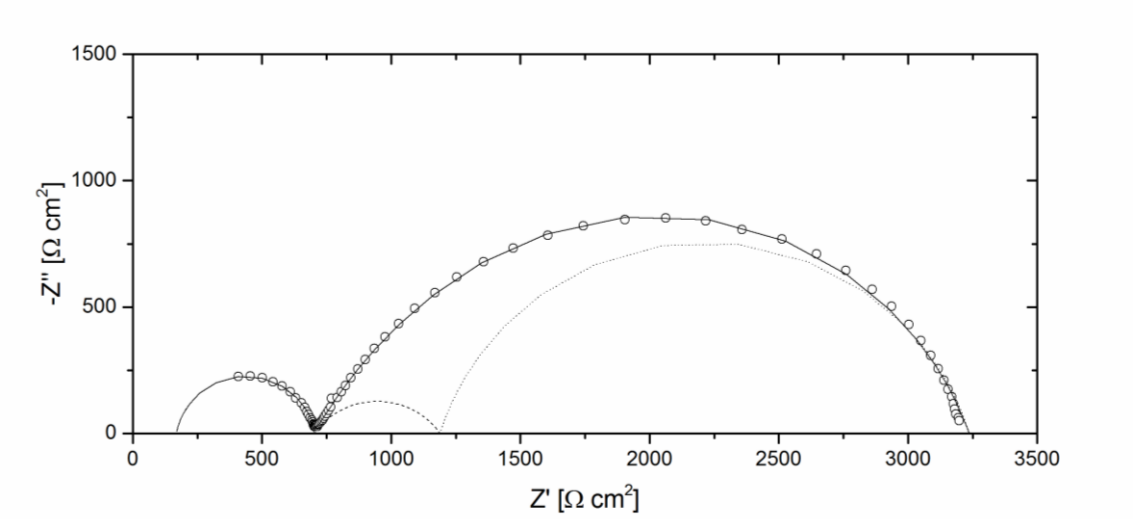

Figure 2. Impedance data (o) for the cell stack with LSCoM electrodes with 5% Co in an atmosphere of 1000 ppm NO +10% O_2 in Ar at 400 °C. The total fit is shown as an unbroken line, and the three arcs are shown with dashed lines.

R_s should be independent of the gas composition but it does show a dependency on the level of Co doping, as seen in figure 1, especially at lower temperatures.

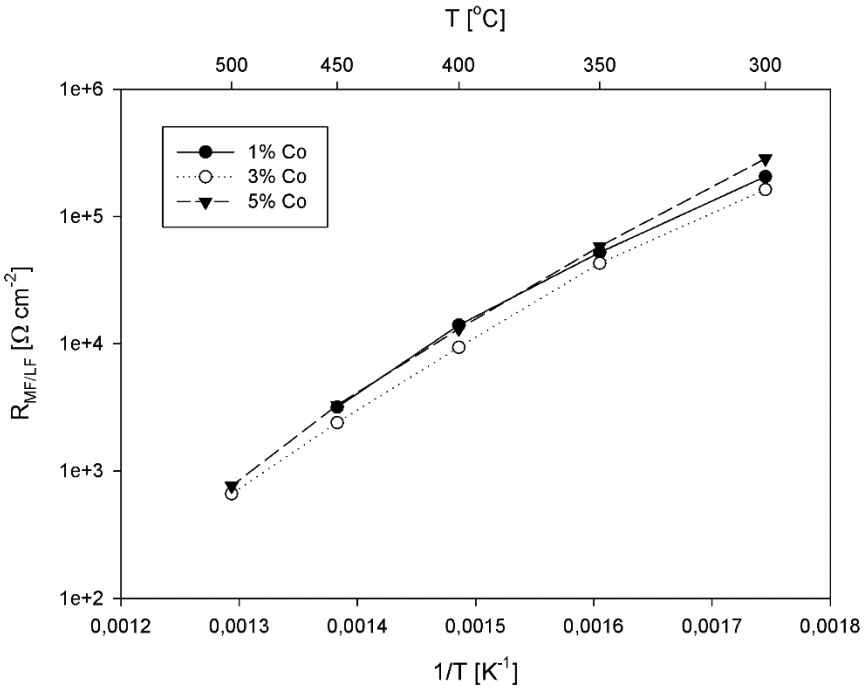

Figure 3. Resistance of the MF and LF arcs for porous cell stacks with LSCoM electrodes with 1% (●), 3% (o) and 5% (▼) Co in 10% O_2 in Ar at 300–500 °C.

Most of the spectra can be fitted with three arcs: high frequency (HF), middle frequency (MF), and low frequency (LF), see Figure 2. However, at 350 to 400 °C, the best fit arises from using only two arcs instead of three. The HF arc remains at all temperatures, but below 350 to 400 °C the MF and LF

arc merge into one arc. It is hard to distinguish whether the MF or LF arc is dominant or if their frequencies overlap so their contributions cannot be separated.

The n-values found for the MF/LF arc at temperatures below 350 °C are closest to those found for the MF arc above 350 °C but a visual inspection suggests that the LF arc becomes the dominant arc whose contribution to the R_p value increases from 500 to 400 °C both in 1000 ppm NO + 10% O_2 in Ar and in 10% O_2 in Ar. The values of EC support both interpretations. For the electrodes with 3% Co, the EC values do seem to support the interpretation that only the MF arc is present for NO at 400 °C and below.

R_{MF+LF} is generally lowest for cell stacks with electrodes with 3% Co, both in an atmosphere containing NO and in the reference atmosphere (figure 3 shows an example). This trend is most noticeable at low temperatures but is also observable at higher temperatures which fits well with the higher E_a values observed for the cells with 3% Co (table 2). In contrast, for the HF arc, the results are more mixed, as the substitution with Co in the electrodes does not have any predictable effect on the HF resistance.

Table 1. E_a for R_p between 250 and 500 °C in 10% O_2 in Ar (E_a R_p O_2) and in 1000 ppm NO + 10% O_2 in Ar (E_a R_p NO).

Electrode	E_a R_p O_2 /eV	E_a R_p NO /eV
LSM/CGO	1.0	0.5
1% Co	0.98	0.89
3% Co	1.06	0.93
5% Co	1.12	0.97

Table 2. E_a for the resistance of the high-frequency arc and the combined middle-to low-frequency arcs between 300 and 500 °C for the backbone.

Electrode	E_a HF O_2 /eV	E_a HF NO /eV	E_a MF/LF O_2 /eV	E_a MF/LF NO /eV
LSM/CGO	0.8	0.8	1.05	0.53
1% Co	1.02	1.00	0.98	0.88
3% Co	1.14	1.17	1.06	0.87
5% Co	1.16	1.15	1.12	0.94

Comparing the resistances measured in 1000 ppm NO + 10% O_2 in Ar with those measured in 10% O_2 in Ar shows that the HF resistances are not strongly affected by the change in atmosphere, while the resistances connected with the MF and LF arcs are generally lower in 1000 ppm NO + 10% O_2 in Ar than in 10% O_2 in Ar (figure 4).

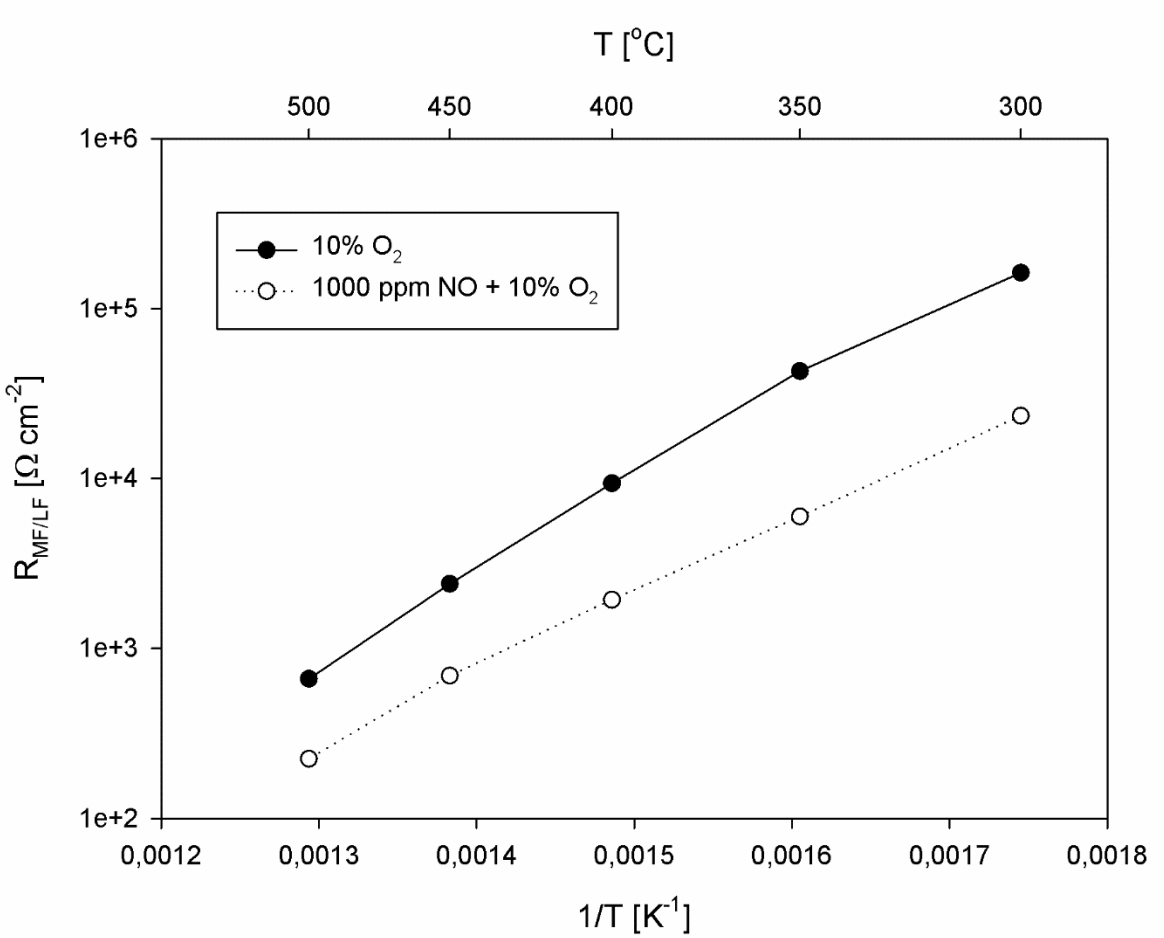

Figure 4. Resistance of the MF and LF arcs for porous cell stacks with LSCoM electrodes with 3% Co in 10% O_2 in Ar (●) and in 1000 ppm NO + 10% O_2 in Ar (o) between 300 and 500 °C.

3.3. Infiltrated cells

Generally, the cells infiltrated with BaO have lower R_p values than the backbone structure, independent of the atmosphere they were measured in as seen in figure 5. The activation energies seem to increase but this is due to the much lower R_p values at the lower temperatures.

For cell stacks with Co, a high-frequency arc is present at all temperatures and it dominates at high temperatures. At 500 °C, it overlaps somewhat with the other arcs but it is clearly distinct at 250–400 °C. It is independent of the atmosphere. E_a appears to be somewhat dependent on the Co doping concentration, with higher E_a values observed with 3 and 5% Co doped into the B-site than for the LSM with 1% Co.

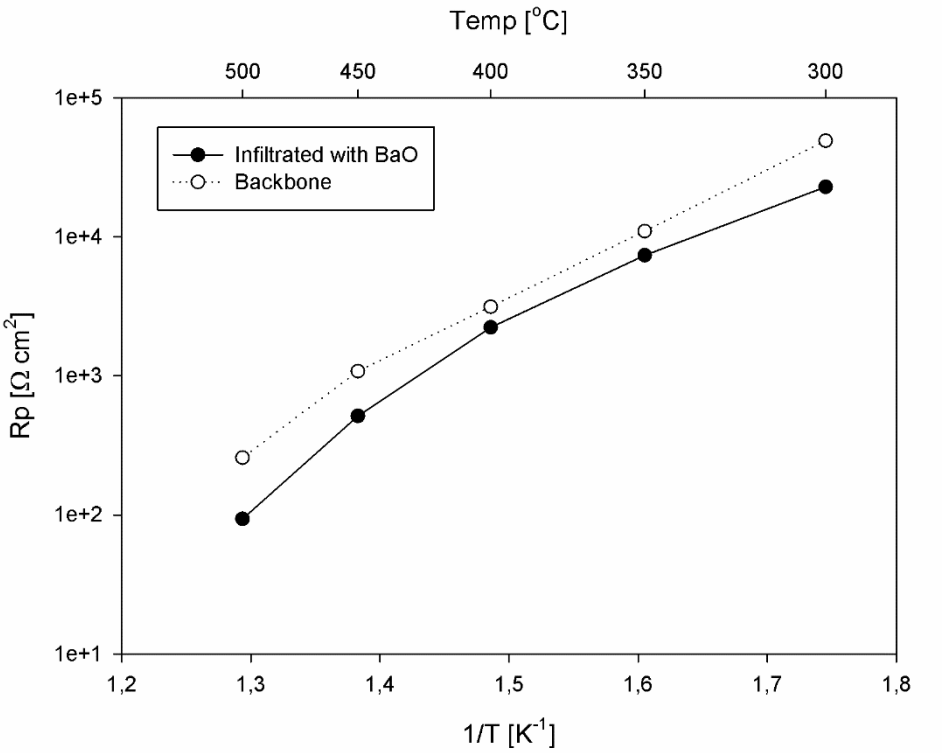

Figure 5. R_p for porous cell stacks with LSCoM electrodes with 5% Co in 1000 ppm NO +10% O_2 in Ar. The temperature range is 300 to 500 °C for the cell stacks infiltrated with BaO (●) and for the backbone structure with no infiltration (o).

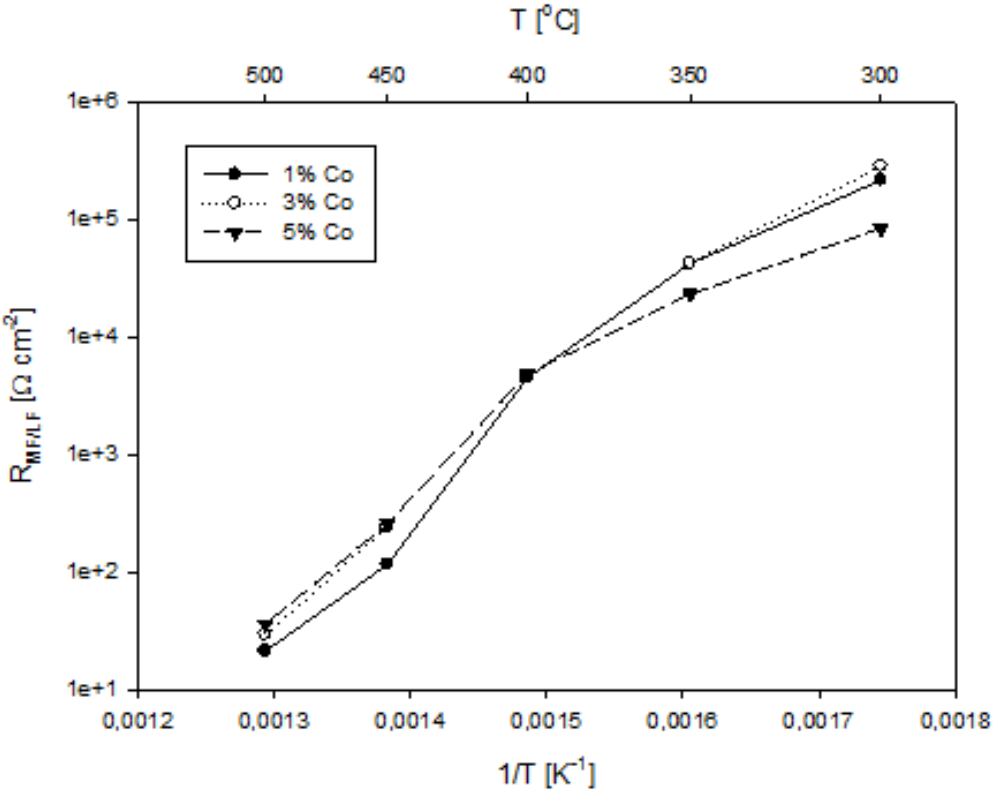

Figure 6. The combined MF and LF resistance arcs for BaO-infiltrated porous cell stacks with 1% Co (●), 3% Co (o) and 5% Co (▼) LSCoM electrodes in an atmosphere of 10% O_2 in Ar between 300 and 500 °C.

For most measurements, two arcs are observed at the middle and low frequencies. These two arcs have close EC values, and it is not possible to separate them at all temperatures, particularly at 250 and 300 °C, when they melt into one large arc. Figure 6 shows the combined MF and LF resistance and that the activation energy shifts at approximately 400 °C, which could be due to a change in which resistance, MF or LF, is dominant. However, both the resistances connected with these arcs and the activation energies depend on the atmosphere, with higher E_a values for an atmosphere of 10% O_2 in Ar than when 1000 ppm NO is present. Additionally, E_a decreases with Co content (table 4).

Table 3. E_a for R_p for cell stacks infiltrated with BaO between 300 and 500 °C.

Electrode	E_a R_p O_2 /eV	E_a R_p NO /eV
LSM/CGO	1.08	1.24
1% Co	1.65	1.15
3% Co	1.71	1.17
5% Co	1.38	1.03

Table 4. E_a for the resistance of the high-frequency arc and the combined middle- to low-frequency arcs between 300 and 500 °C for cell stacks infiltrated with BaO.

Electrode	E_a HF O_2 /eV	E_a HF NO /eV	E_a MF/LF O_2 /eV	E_a MF/LF NO /eV
LSM/CGO	1.11	0.80	1.54	1.47
1% Co	1.12	1.15	1.84	1.34
3% Co	1.29	1.40	1.79	1.22
5% Co	1.27	1.33	1.50	1.08

At 450–500 °C, cell stacks doped with Co show an extra LF arc with a high EC that is present in both an atmosphere with 1000 ppm NO + 10% O_2 in Ar and one with only 10% O_2 in Ar, see figure 7 for an example. However, the arc shifts to higher values when no NO is present.

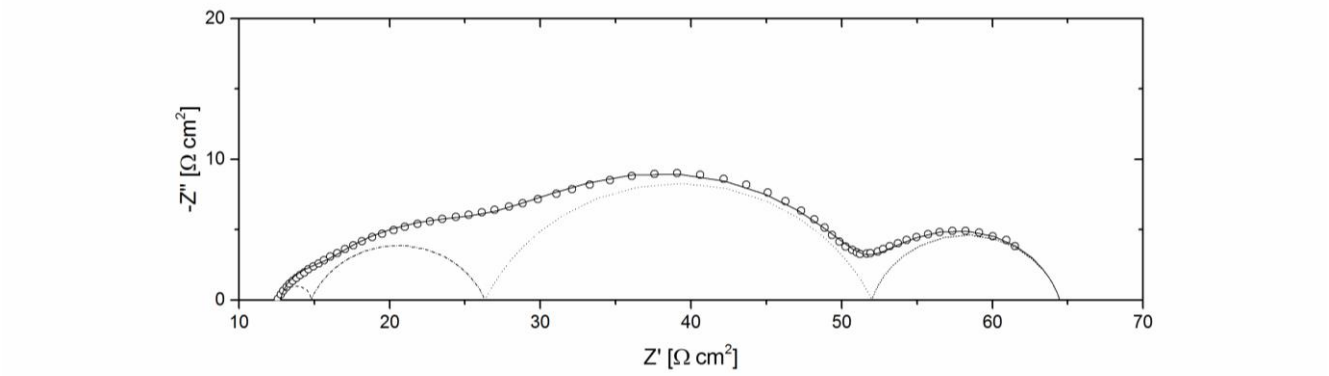

Figure 7. Impedance data (o) for the cell stack with 5% Co LSCoM electrodes in an atmosphere of 10% O_2 in Ar at 500 °C. The total fit is shown as an unbroken line, and the four arcs are shown with stippled lines.

The resistance of the HF arc is independent of the atmosphere, although the values may be slightly lower for the measurements in 1000 ppm NO + 10% O_2 in Ar. At temperatures below 450 °C, the resistances of the MF and LF arcs are generally lower with 1000 ppm of NO present, but at 500 °C the measurements in 10% O_2 in Ar have the lowest resistance.

3.4. Infiltration with LSM

The effect of further infiltration with LSM15 in cell stacks with 1% Co infiltrated with BaO was analyzed by comparing EIS measurements.

Since the porous cell stack was submerged in the precursor solution during infiltration, the LSM formed will be present in both the electrodes and the electrolyte phase. LSM15 has electronic conductivity and can short circuit the cell stack at higher temperatures. Additionally, the R_s values are remarkably lower for the cell stack infiltrated with both BaO and LSM between 400 and 500 °C.

The R_p values are also lower for the cell infiltrated with LSM at temperatures above 350 °C. In particular, the step from 350 to 400 °C decreases the R_p values substantially more for the cell infiltrated with LSM than those of the cells without LSM. The ratio between the R_p values in 10% O_2 in Ar and in 1000 ppm NO + 10% O_2 in Ar, hereafter called R_{NO}/R_{O2}, shows that the resistance of cells infiltrated with LSM increase quicker in an atmosphere containing NO than in an atmosphere with O_2 (figure 8).

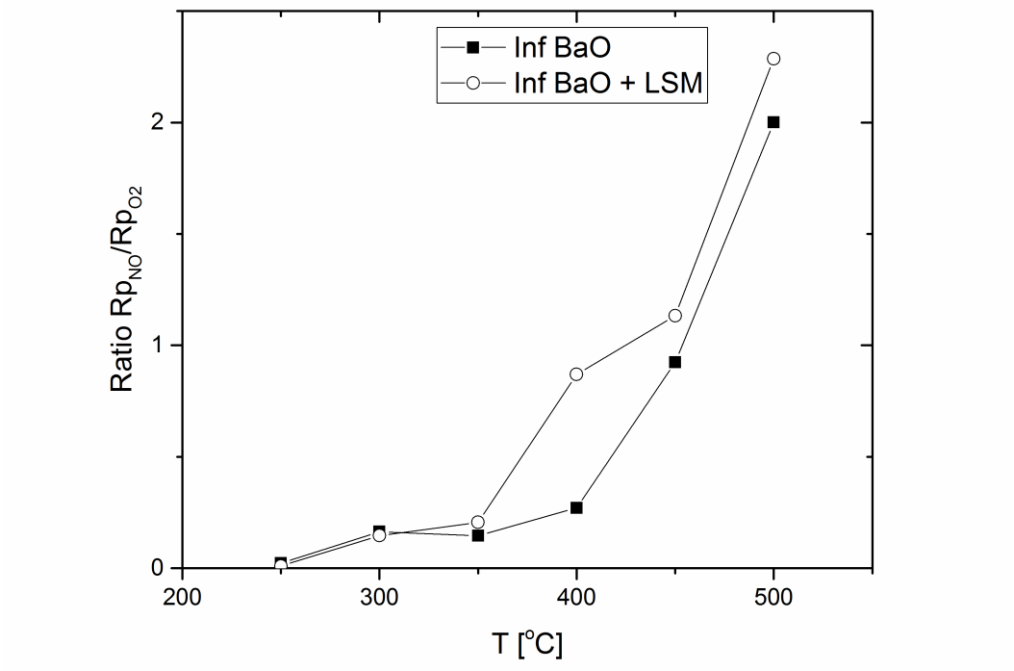

Figure 8. Ratio between R_p in 1000 ppm NO + 10% O_2 and R_p in 10% O_2 in Ar for cell stacks infiltrated with BaO (▪) and BaO + LSM15 (○) between 250 and 500 °C.

If the R_p values are divided into contributions from R_{HF} and R_{MF} + R_{LF} it is clear that the infiltration with LSM15 affects only R_{MF} + R_{LF} and not R_{HF}.

3.5. EIS during polarization

EIS spectrograms were also recorded during polarization of the cell stacks doped with either 1% or 5% Co and infiltrated with BaO at 400 °C. The cell stacks were subjected to EIS under polarizations in the following order: +3 V, -3 V, +5 V, -5 V, +7 V, -7 V, with one hour of restitution at OCV between each polarization step.

R_s and R_{HF} are independent of the polarization. R_p decreases with increasing polarization, as illustrated in figure 9.

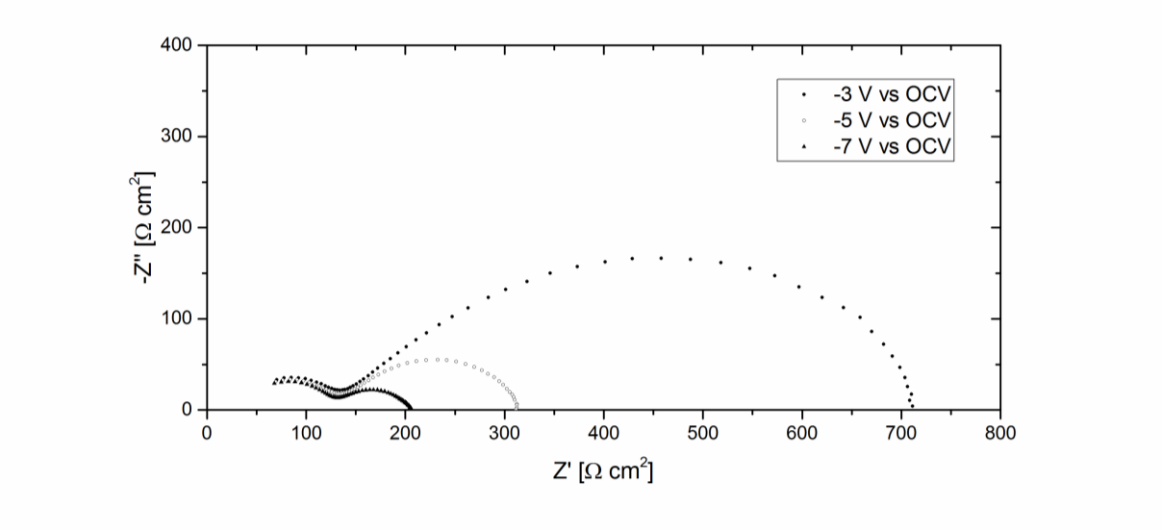

Figure 9. EIS spectra during polarization with +3 (▪), +5 (○) and +7 V (●) vs OCV for a cell stack with LSCoM electrodes with 5% Co at 400 °C in 1000 ppm NO + 10% O_2 in Ar.

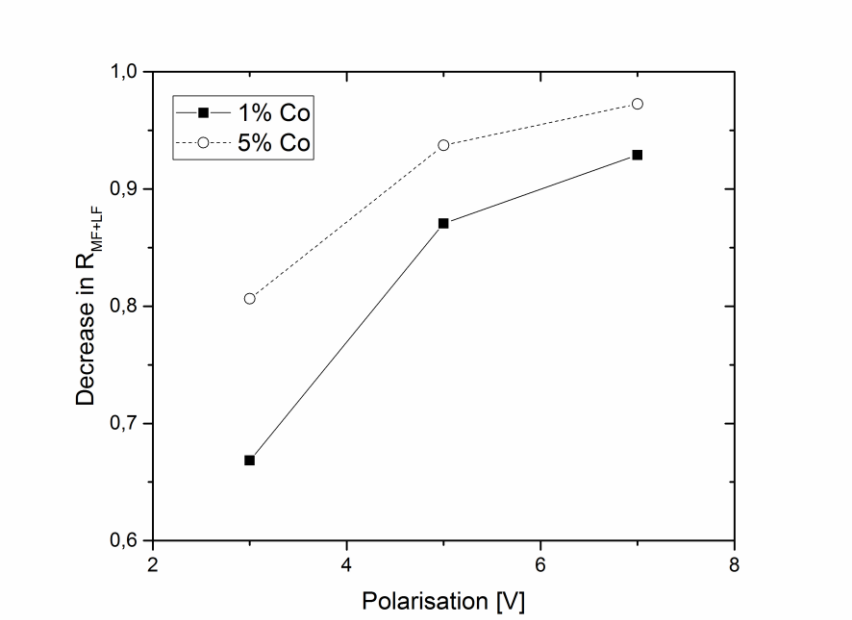

Figure 10. Decrease in $R_{MF} + R_{LF}$ as a function of the polarization of cell stacks with LSCoM electrodes with 1% (▪) and 5% (○) Co at 400 °C in 1000 ppm NO + 10% O_2 in Ar polarized at +3, +5 and +7 V vs OCV.

With polarizations of ±3 V and ±5 V, R_{MF} + R_{LF} are generally slightly larger under negative polarization than under positive polarization. This tendency was not observed at ±7 V. The decrease in R_{MF} + R_{LF} during polarization is slightly larger for the cell stacks with 5% Co than for the ones with 1% Co (figure 10).

3.6. Variation of NO concentration

The concentration of NO was varied between 500, 1000 and 2000 ppm NO in 10% O_2 + Ar to test the cell stacks with 1 and 5% Co at 400 °C. For both levels of Co doping, R_{LF} decreases with increasing NO concentration, while R_{MF} decreases with NO concentration only for cells with 5% Co. For those with 1% Co, it appears to be independent of the NO concentration, but the EC values suggest that this could be due to mixing of the MF and LF resistances, as the EC value decreases from 500 to 1000 ppm but increases from 1000 to 2000 ppm for the MF resistance of the 5% Co cell stacks. Otherwise, the EC values generally decrease with increasing NO concentrations, except for the HF case, whose EC and resistances are both independent of the NO concentration.

Table 5. Resistances for porous cell stacks doped with 1 and 5% Co in NO concentrations varying between 500, 1000, and 2000 ppm at 400 °C.

NO /ppm	1% Co				5% Co			
	R_{HF} /Ω cm^{-2}	R_{MF} /Ω cm^{-2}	R_{LF} /Ω cm^{-2}	R_{ULF} /Ω cm^{-2}	R_{HF} /Ω cm^{-2}	R_{MF} /Ω cm^{-2}	R_{LF} /Ω cm^{-2}	R_{ULF} /Ω cm^{-2}
500	5,4E+01	2,9E+02	1,2E+03	9,6E+02	4,4E+01	8,7E+01	4,8E+02	9,8E+02
1000	5,3E+01	2,2E+02	1,0E+03	6,4E+02	3,9E+01	6,6E+01	3,9E+02	6,6E+02
2000	5,9E+01	1,3E+02	4,2E+02	1,2E+03	5,1E+01	1,2E+02	3,7E+02	3,1E+02

4. DISCUSSION

The high-frequency arc does not depend on the atmosphere or polarization but it does depend on the concentration of Co. It typically has E_a values of approximately 0.8–1.2 eV which indicates that the process is not related to diffusion or gas conversion but instead is more likely related to the electrolyte or to the transfer of oxide ions at the electrode-electrolyte interface [20]. Co is known as a sintering aid [21] and a visual inspection suggested that the diameter of the sintered button cells decreases with increasing Co content, revealing that Co also affects the microstructure, making the cell stack denser.

The middle- and low-frequency processes, which are hard to separate, are dependent on the polarization with decreasing values at increasing polarizations, particularly for the LF arc. They also depend on the atmosphere; the E_a values are lower in NO than in O_2. In a previous study, the middle-frequency arc was attributed to surface diffusion, adsorption, or the transfer of oxide ions from the LSM

to the CGO [22]. This attribution may also fit the two arcs observed here; the E_a value should be approximately 1.5–2.0, which is true for the measurements in 20% O_2 in Ar. Furthermore, these arcs also decrease in size with increased NO concentration which implicates surface diffusion and adsorption.

Figure 6 suggests that the dominating contribution shifts at approximately 400 °C. When the temperature decreases the ionic conductivity of the metal oxides, which is probably the limiting factor for the cells, decreases as well. This suggests that the part of R_{MF+LF} coming from the transfer of oxygen ions from the electrode to the electrolyte becomes the major contributor to the resistances at temperatures below 400 °C.

Infiltrating with LSM decreases R_{MF+LF} but not R_{HF}. It was expected that infiltration with LSM15 would make the electrodes more active, both because LSM is electrocatalytically active in the reduction of NO [23] and because the nanoparticles of LSM formed during infiltration can be more active than the LSM bulk phase in the backbone that was sintered at 1200 °C. Furthermore, LSM has good electronic conductivity that can add to the activity of the electrodes. Thus, the decrease in R_{MF+LF} could be due to better adsorption onto the large surface area provided by the LSM nanoparticles.

One more arc type, an extremely low-frequency arc, is observed, predominantly above 400 °C. Since it has a relatively high n value of more than 0.9, it could be identical to the low-frequency arc found in [22] which was a type of conversion arc related to the cells reacting electrochemically with an intermediate (possible NO_2) instead of NO. In this case, this arc does not dominate the spectra, possibly because the concentration of the intermediate is relatively high because of the presence of 10% O_2 and the ability of Co-doped perovskites to catalytically form NO_2 [24]. However, the very low-frequency arcs are also seen for some of the measurements without any NO in the atmosphere, so it could be a different low-frequency arc. Because it has a higher EC value, it may be a diffusion arc arising from the electrodes reacting with O_2.

A previous report showed that the addition of Co increases the activity of the cell stacks with respect to the conversion of NO_x to N_2 [15] which was attributed to an increased catalytic activity of the electrodes in combination with an increased electrical conductivity. The impedance study revealed that doping with Co also strongly affects the resistance of both the backbone and the infiltrated electrodes.

The resistance of the electrolyte increased as the Co doping level increases. This is surprising because the Co should only be present in the electrodes, but some of the Co may migrate to the boundary layer during sintering, possibly forming less conductive layers. From this perspective, doping with only 1% Co is preferable as it results in the lowest R_s.

E_a and R_{MF+LF} also depend on the level of Co doping. E_a decreases with increasing Co doping while the lowest values for R_{MF+LF} are observed with 3 and 5% Co. This may be due to the catalytic activity of the Co-doped perovskites and possibly to the increased electronic conductivity. The previous study showed that the conversion degree depends not on the level of Co doping but only on whether Co was present, possibly because the effects of the increased R_s mitigated those of the decreased R_{MF+LF}.

Generally, the resistances for the infiltrated cell stacks are lower than those for the pure backbone. This is the case for HF, MF, and LF. However, these resistances do depend on the temperature and the level of Co doping. The difference between the MF+LF resistances of the backbone and of the BaO infiltrated cells is larger at high temperatures. For the cell stacks with 1% Co in the electrodes, the resistances of the MF and LF process are unrelated to infiltration at temperatures of 350 °C and below.

This is not observed for the cell stacks with electrodes with 5% Co. Traulsen [12] suggested that both the MF and the LF arcs of the cell stacks infiltrated with BaO are related to a triple phase boundary process and that BaO can form Ba(NO_3) from reactions with NO_2 in a catalytic and non-electrochemical process. The electrochemical impedance from this process should arise from the availability of O^-/O(ads) species to form NO_3(ads) from NO_2 and from the transfer across the triple phase boundary.

The electrodes with 5% Co should have a higher catalytic activity toward forming NO_2, but in fact all the cell stacks with Co doping have similar catalytic activity. This might be due to the relatively small doping. The addition of Co could increase the ionic conductivity, affecting the availability of oxygen surface species needed for the formation of NO_3(ads) from NO_2.

5. CONCLUSION

Impedance spectra were recorded in O_2/Ar atmospheres with or without NO between 250 and 500 °C. The resulting impedance data were then fitted with equivalent circuits; it was necessary to use between two and four subunits to obtain a suitable fit.

Infiltration with BaO decreased the resistances of the cells and additional infiltration with LSM further increased the activity.

Generally, the resistances were lower in an atmosphere containing NO_x than in an atmosphere with only O_2 and Ar which is preferable as this indicates selectivity of the electrodes towards NO_x.

Increasing the NO concentration decreased the part of R_p attributed to the absorption or transfer of electrons across boundaries; similar results were obtained by recording the impedance spectra under polarization. This could be the result of better adsorption due to a higher reactant concentration or to increased activity of the electrodes.

The level of Co doping affected the resistance of the electrodes, and increasing the Co doping decreased R_{MF+LF} and E_a in NO containing atmosphere. This could be due to the increased catalytic activity and electric conductivity of the electrodes.

ACKNOWLEDGEMENTS
This research was funded by the Danish Strategic Research Council, project 09-065186.

References

1. S. Matsumoto, *Catal. Today*, 29 (1996) 43
2. S. Pancharatnam, R. A. Huggins and D. M. Mason, *J. Electrochem. Soc*., 122 (7) (1975) 869
3. D. C. Cicero and L. A. Jarr, *Sep. Sci. Technol*., 25 (1990) 13
4. T. Hibino, *J. Appl. Electrochem*., 25 (1995) 203
5. G. Reinhardt, H.-D. Wiemhöfer and W. Göpel, *Ionics*, 1 (1995) 32
6. S. Bredikhin, K. Maeda and M. Awano, *Ionics,* 7 (2001) 109
7. K. K. Hansen, H. Christensen and E. Skou, *Ionics*, 6 (2000) 340
8. S. Park, H. S. Song, H. J. Choi and J. Moon, *Solid State Ionics*, 175 (2004) 625

9. Y. Tong, B. Zhao, T. Yang, F. Yang, Q. Hu, C. Zhao, *Int. J. Electrochem. Sci.*, 10 (2015) 5338
10. S. J. Muthiya, S. Pachamuthu, *Int. J. Green Energy*, 15(5) (2018) 314
11. R. M. L. Werchmeister, K. K. Hansen and M. Mogensen, *Mat. Res. Bull*., 45 (2010) 1554
12. M. L. Traulsen, K. B. Andersen and K. Kammer Hansen, *J. Mater. Chem*., 22 (2012) 11792
13. Y. Bai, M. Liu, D. Ding, K. Blinn, W. Qin, J. Liu and M. Liu, *J. Power Sources*, 205 (2012) 80
14. R. V. Wandekar, B. N. Wani and S. R. Bharadwaj, *Solid State Sci*., 11 (2009) 240
15. R. M. L. Werchmeister, J. J. Bentzen, K. B. Andersen and K. Kammer Hansen, *J. Electrochem. Soc.*, 161 (2014) H663
16. L. A. Chick, L. Pederson, G. Maupin, J. Bates, L. Thomas and G. Exarhos, *Mater. Lett*., 10(1,2) (1990) 6
17. B. A. Boukamp, *Solid State Ionics,* 20 (1986) 31
18. E. Barsoukov and J. R. MacDonald, Impedance spectroscopy - Theory, Experimental and Applications, 2nd Edition, Wiley Interscience, New York (2005)
19. T. Jacobsen, B. Zachau-Christensen, L. Bay and S. Skaarup, Proc. 17th risø int. symp. on materials science, no. 17, p. 29, Risø National Laboratory, Roskilde, Denmark (1996)
20. M. J. Jørgensen and M. Mogensen, *J. Electrochem. Soc.,* 148 (2001) A433
21. D. P. Fagg, J. C. C. Abrantes, D. Pérez-Coll, P. Núñez, V. V. Kharton and J. R. Frade, *Electrochim. Acta,* 48 (2003) 1023
22. R. M. L. Werchmeister, K. Kammer Hansen and M. Mogensen, *J. Electrochem. Soc*., 157(5) (2010) P35
23. E. D. Wachsman, P. Jayaweera, G. Krishnan, and A. Sanjurjo, *Solid State Ionics*, 136–137 (2000) 775
24. C. H. Kim, G. Qi, K. Dahlberg and W. Li, *Science*, 327 (2010) 1624